Received: xxx **Accepted:** xxx **Published:** xxx.
DOI. xxxxxxx
Volume xxx, Issue xxx, p.p. 1-33: xxx
Research Article

Open Access

Control and Optimization in Applied Mathematics - COAM

Block-Wise Multi-Objective Binary Control of HIV Treatment: Synchronous and Asynchronous Control Strategies

Islem Bennadja[1] ✉, **Omar Kebiri**[2], **Djamal Chaabane**[1]

[1] Laboratory AMCD & RO, Department of Operational Research, Faculty of Mathematics, University of Science and Technology Houari Boumediene (USTHB), Algiers, Algeria.
[2] Department of Stochastics and its Applications, Institute of Mathematics, Brandenburg University of Technology Cottbus-Senftenberg (BTU), Cottbus, Germany.

✉ **Correspondence:**
Islem Bennadja
E-mail:
ibennadja@usthb.dz

How to Cite
Bennadja, I., Kebiri, O., Chaabane, D. (2026). "Block-wise multi-objective binary control of HIV treatment: Synchronous and asynchronous control strategies". *Control and Optimization in Applied Mathematics*, X(x), 1-33. https://doi.org/10.30473/coam.2026.75678.1341

Abstract. Human immunodeficiency virus (HIV) gradually depletes $CD4^+$ T-cells, weakening the immune system and potentially leading to AIDS without effective treatment. To counter this immune decline, antiretroviral therapy (ART) has greatly improved the clinical management of HIV by suppressing viral replication and preserving immune function. However, because treatment is often required over long periods, its use may be limited by cumulative toxicity, drug resistance, and adherence challenges. These limitations have encouraged the study of structured treatment interruptions, in which therapy is temporarily stopped and resumed according to a planned schedule to reduce drug exposure while maintaining viral control. In this context, this work proposes a clinically motivated block-wise multi-objective optimization framework for HIV treatment scheduling, based on a nonlinear six-state dynamical model with two binary control variables corresponding to protease inhibitor (PI) and reverse transcriptase inhibitor (RTI) therapies. Rather than determining a single treatment schedule over the entire time horizon, the proposed framework incorporates sequential re-optimization over consecutive 30-day blocks to reflect periodic clinical reassessment and treatment adaptation. The study also compares asynchronous and synchronous binary control strategies under identical conditions. Within each block, daily treatment decisions are optimized using the Non-dominated Sorting Binary Genetic Algorithm II (NSBGA-II), with the aim of preserving $CD4^+$ T-cell levels, suppressing viral load, and reducing total drug administration. This formulation provides a more clinically realistic basis for constructing adaptive and personalized HIV treatment schedules.

Keywords. Multi-objective optimization, Binary optimal control, HIV, ART scheduling.

MSC. 90C29; 49N90; 93C15.

1 Introduction

HIV is a chronic infection that directly attacks the immune system, progressively destroying $CD4^+$ cells. Without treatment, it leads to AIDS, leaving the patient vulnerable to numerous opportunistic infections. The global challenge posed by Human Immunodeficiency Virus (HIV) [16] continues to drive the search for effective, long-term treatment strategies capable of preserving immune function while limiting the burden of therapy.

In this context, structured treatment interruptions (STIs) have been proposed [1, 10, 14, 21]. These consist of an initial period of continuous therapy, followed by planned treatment breaks aimed at reducing drug exposure while maintaining sufficient viral control. From a control perspective, ART scheduling under STIs can be formulated as a multi-objective binary optimal control problem, where daily treatment decisions are either "on" (drug administered) or "off" (drug withheld). The aim is to balance several conflicting goals, namely preserving immune function, suppressing viral load, and reducing treatment burden. These goals are captured through three objective functions.

To formulate the optimization problem, we rely on mathematical models that describe HIV progression. Early models, based on three differential equations, represented the interaction between healthy cells, infected cells, and free virus particles [12]. These were later enriched with the incorporation of cytotoxic T-lymphocytes (CTLs) [19] and, more recently, the inclusion of viral aggressiveness and the direct effects of treatments, leading to the advanced six-equation model in [9], which we adopt in this work.

Building on this HIV model, the present study investigates block-wise multi-objective optimization of binary ART schedules under periodic clinical reassessment. Rather than determining a treatment plan once over the entire horizon, the total treatment period of 1500 days is decomposed into successive 30-day blocks, and treatment decisions are updated from one block to the next according to the patient's evolving physiological state. Optimization begins when the $CD4^+$ count falls below the clinical threshold of 350 cells/µL, marking the initiation of ART.

Within each block, daily treatment decisions are binary, meaning that each drug is either administered (1) or withheld (0). These decisions are optimized using the Non-dominated Sorting Binary Genetic Algorithm II (NSBGA-II) a binary-chromosome adaptation of NSGA-II [5] as implemented in [17]. However, the contribution of the present work does not lie in introducing a new optimization algorithm itself, but in reformulating the treatment decision process in a block-wise manner so that therapy can be re-evaluated and updated sequentially over time. The final state of one block becomes the initial state of the next, and the remaining days at the end of the horizon are also incorporated into the optimization procedure.

We further examine two binary control strategies under the same modeling and optimization framework:

1. **Asynchronous control**, in which PI and RTI are scheduled independently, offering greater flexibility in treatment adjustment;

2. **Synchronous control**, in which both drugs are administered or withheld simultaneously, simplifying treatment and potentially improving patient adherence.

Their comparison constitutes an additional contribution of this work, since it makes it possible to evaluate how the structure of treatment decisions influences the resulting schedules and objective trade-offs under identical conditions.

The remainder of the paper is structured as follows. In Section 2, we review the mathematical progression from foundational HIV models to the extended six-state system used in this study and establish positivity and boundedness of solutions. Section 3 formulates the multi-objective optimal control problem and justifies the choice of NSBGA-II. Section 4 presents the numerical implementation and the main optimization results under asynchronous and synchronous control. Section 5 reports supplementary sensitivity and robustness analyses. Finally, conclusions and future directions are discussed in Section 6.

2 Mathematical Models for HIV Infection

A foundational approach to modeling the in-host dynamics of HIV infection is presented in [12], where the system tracks three state variables: healthy CD4$^+$ T-cells, infected CD4$^+$ T-cells, and free virus particles, within a whole-body framework. The model assumes constant influx and natural death of healthy T-cells, infection driven by virus-cell interactions, and viral production from infected cells. Mathematically, the dynamics are given by:

$$\begin{cases} \dot{x} = \lambda - dx - \beta xv, \\ \dot{y} = \beta xv - ay, \\ \dot{v} = ky - \tau v. \end{cases} \tag{1}$$

In this model, we look at the concentrations of three key components: healthy CD4$^+$ T-cells x, infected CD4$^+$ T-cells y, and free virions v. The natural regeneration rate of CD4$^+$ T-cells is denoted by λ, while d represents the death rate of healthy CD4$^+$ T-cells. On the other hand, a is the death rate of infected CD4$^+$ T-cells. The infection rate, or how quickly healthy cells become infected, is represented by β. We also have k, which is the production rate of virions per infected cell, and τ, which is the natural clearance rate of free virions.

To better understand how the immune system works, Wodarz and Nowak extended the basic model in [19] by incorporating cytotoxic T-lymphocyte (CTL) dynamics. The expanded system introduces two additional compartments: CTL precursors (w) and CTL effectors (z), capturing

their proliferation, differentiation, and virus suppression functions. The model is formulated as:

$$\begin{cases} \dot{x} = \lambda - dx - \beta xv, \\ \dot{y} = \beta xv - ay - pzy, \\ \dot{v} = ky - \tau v, \\ \dot{w} = cxyw - cqyw - bw, \\ \dot{z} = cqyw - hz, \end{cases} \tag{2}$$

where CTL precursors proliferate with rate $cxyw$, differentiate into effectors at rate $cqyw$, and decay with rate bw, while CTL effectors decay at rate hz. The immune-mediated clearance of infected cells is accounted for by an additional term $-pzy$.

To more realistically capture disease progression and therapeutic intervention, a further extension was proposed in [9], where the infection rate constant β is replaced by a time-evolving state variable r, interpreted as a marker of viral aggressiveness. Moreover, the administration of antiretroviral treatments is modeled using binary control variables η_P and η_R, which indicate whether protease inhibitors (PI) and reverse transcriptase inhibitors (RTI) are applied, respectively. The efficacy of each treatment is represented by the parameters u_P and u_R, which quantify the intensity of the protease inhibitor and reverse transcriptase inhibitor effects when activated. These therapies modulate the infection and viral production processes. The model employed in this study corresponds to the version proposed in [9]:

$$\begin{cases} \dot{x} = \lambda - dx - rxv, \\ \dot{y} = rxv - ay - pyz, \\ \dot{w} = cxyw - cqyw - bw, \\ \dot{z} = cqyw - hz, \\ \dot{v} = k(1 - u_P\eta_P)y - \tau v, \\ \dot{r} = r_0 - u_R\eta_R. \end{cases} \tag{3}$$

This formulation reflects both the immune system response and the impact of therapeutic strategies aimed at suppressing viral replication and limiting disease progression.

The model incorporates several parameters that must be specified for numerical simulations. A summary of the parameter descriptions, numerical values, and units is provided in Table 1. These descriptions and values are sourced from [9]. This study is entirely simulation-based and does not use real patient data. Therefore, ethical approval and informed consent are not required.

Dimensional consistency for $\dot{r} = r_0 - u_R\eta_R$ is maintained as u_R and r_0 share the units copies^{-1} mL day^{-2}. Thus, the net rate $r_0 - u_R = 10^{-10}$ carries these units, representing the suppressed growth intensity of infectivity.

Table 1: Description and values of parameters used in the HIV model.[1]

Parameter	Description	Value / Unit
λ	Production rate of healthy CD4$^+$ T cells from the source	7 cells μL^{-1} day^{-1}
d	Natural death rate of healthy CD4$^+$ T cells	7×10^{-3} day^{-1}
a	Death rate of infected CD4$^+$ T cells	0.0999 day^{-1}
p	Elimination rate of infected cells by CTL effectors	2 μL cells^{-1} day^{-1}
c	Proliferation rate of CTL precursors	5×10^{-6} μL^2 cells^{-2} day^{-1}
q	Activation threshold for converting CTL precursors into CTL effectors	120 cells μL^{-1}
b	Death rate of CTL precursors	0.017 day^{-1}
h	Death rate of CTL effectors	0.06 day^{-1}
k	Virus production rate per infected cell	300 copies mL^{-1} cells^{-1} day^{-1}
τ	Natural clearance rate of free virus particles	0.2 day^{-1}
r_0	Viral infectivity rate (growth intensity)	10^{-9} copies^{-1} mL day^{-2}
u_P	Dosage of protease inhibitors (PI), reducing virion maturation	0.7
u_R	Dosage of reverse transcriptase inhibitors (RTI), blocking new infections	9×10^{-10} copies^{-1} mL day^{-2}

Before introducing the optimization framework, we first verify that system (3) is well posed and biologically meaningful.

2.1 Positivity and Boundedness of Solutions

Proposition 1. For any measurable binary controls $\eta_P(t), \eta_R(t) \in \{0, 1\}$ and any nonnegative initial condition

$$X(0) = (x(0), y(0), w(0), z(0), v(0), r(0)) \in \mathbb{R}^6_+,$$

the solution of system (3) exists uniquely for all $t \geq 0$ and all state variables remain nonnegative and bounded on every finite time interval.

Proof. Positivity follows by evaluating the vector field of system (3) on the boundary of $\mathbb{R}^6_+$. Indeed, if $x = 0$ then $\dot{x} = \lambda > 0$; if $y = 0$ then $\dot{y} = rxv \geq 0$; if $w = 0$ then $\dot{w} = 0$; if $z = 0$ then $\dot{z} = cqyw \geq 0$; if $v = 0$ then $\dot{v} = k(1 - u_P\eta_P(t))y \geq 0$; and if $r = 0$ then $\dot{r} = r_0 - u_R\eta_R(t) \geq 0$. Hence $\mathbb{R}^6_+$ is positively invariant.

To prove boundedness, note that, since all states are nonnegative,

$$\dot{x} = \lambda - dx - rxv \leq \lambda - dx.$$

A comparison argument yields

$$0 \leq x(t) \leq \max\left\{x(0), \frac{\lambda}{d}\right\}.$$

Furthermore, $\dot{r} = r_0 - u_R\eta_R(t)$. Since $\eta_R(t) \in \{0, 1\}$, the RTI term u_R actively suppresses the rate of increase in viral aggressiveness. Consequently, $r(t)$ is bounded within $[r(0) + (r_0 -$

$u_R)t, r(0) + r_0 t]$, remaining biologically meaningful and bounded on any finite interval. Using these bounds in the (y, v) equations shows that their growth is controlled by the linear decay terms $-ay$ and $-\tau v$, and hence $y(t)$ and $v(t)$ remain finite. The equations for $w(t)$ and $z(t)$ then have bounded coefficients, so $w(t)$ and $z(t)$ are also bounded. Therefore all components of the solution remain bounded on every finite time interval. □

3 Multi-Objective Optimal Control Problem

In this section, HIV therapy design is formulated as a multi-objective binary optimal control problem. We consider a nonlinear system of six differential equations describing the within-host dynamics of HIV infection (see Section 2). The *state vector* is defined as:

$$X(t) = (x(t), y(t), w(t), z(t), v(t), r(t)) \in \mathbb{R}^6_+, \quad \forall t \in [t_0, t_f],$$

where the biological meanings of the state variables are as follows:

- $x(t)$: healthy CD4$^+$ T-cells,
- $y(t)$: infected CD4$^+$ T-cells,
- $w(t)$: precursor cytotoxic T-lymphocytes (CTLs),
- $z(t)$: effector CTLs,
- $v(t)$: free virus particles,
- $r(t)$: viral aggressiveness.

The *binary control variables* represent structured on-off drug administration:

$$\eta(t) = (\eta_P(t), \eta_R(t)), \quad \eta_P(t), \eta_R(t) \in \{0, 1\}, \quad \forall t \in [t_0, t_f],$$

where:

- $\eta_P(t) = 1$ indicates the application of the protease inhibitor (PI), while $\eta_P(t) = 0$ indicates no administration of the PI.
- $\eta_R(t) = 1$ indicates the application of the reverse transcriptase inhibitor (RTI), while $\eta_R(t) = 0$ indicates no administration of the RTI.

Drug effects enter the system through the modification of key terms in the ODEs:

- PI reduces the viral production term via a factor $(1 - u_P \eta_P(t))$,

- RTI suppresses viral replication by reducing the infection rate via $\dot{r}(t) = r_0 - u_R \eta_R(t)$.

Let $\mathcal{E}$ denote the set of admissible binary control functions defined over $[t_0, t_f]$, measurable and taking values in $\{0, 1\}$. Given a control pair $\eta(t) \in \mathcal{E}$, the system evolves from an initial state $X(t_0)$, producing a trajectory $X(t)$ through numerical simulation.

$$\mathcal{E} = \{(\eta_P, \eta_R) \mid \eta_P(t), \eta_R(t) \in \{0, 1\}, \text{ measurable over } [t_0, t_f]\}. \tag{4}$$

3.1 Objective Functions

The objective functions are expressed in discrete form, where the time step corresponds to days in the discretized version of system (3).

Objective function 1 – Immune Preservation

This objective function aims to sustain a high level of healthy $CD4^+$ T-cells over the treatment horizon, ensuring a strong immune system. To express this goal within a minimization framework, it is defined as the negative cumulative $CD4^+$ T-cell count.

$$I_1(\eta) = -\sum_{t=t_0}^{t_f} x(t). \tag{5}$$

Objective function 2 – Viral Suppression

This objective function aims to reduce the viral burden by minimizing the cumulative viral load over the treatment horizon. Lower values of this objective correspond to stronger suppression of HIV replication.

$$I_2(\eta) = \sum_{t=t_0}^{t_f} v(t). \tag{6}$$

Objective function 3 – Treatment Burden

This objective function penalizes the overall treatment burden induced by the applied therapy schedule. It is defined through the cumulative drug administration over the treatment horizon.

$$I_3(\eta) = \sum_{t=t_0}^{t_f} (\eta_P(t) + \eta_R(t)). \tag{7}$$

The three objective functions in our study are defined separately to preserve their distinct clinical meanings. Immune preservation, viral suppression, and treatment burden correspond to different therapeutic goals, and reducing them to a single aggregated criterion would mask the natural conflicts between them. Their separate formulation therefore allows the optimization framework to explore clinically relevant trade-offs and identify Pareto-optimal treatment schedules.

3.2 Optimization Problem Statement

The objective of this study is to identify structured treatment schedules that achieve a balance between therapeutic effectiveness and the preservation of immune health. To guarantee the clinical relevance of the generated schedules, we impose a state-path constraint on the healthy CD4$^+$ T-cell count:

$$x(t) \geq 500\,\text{cells}/\mu\text{L}, \quad \forall t \in [t_0, t_f]. \tag{8}$$

This constraint is motivated by clinical considerations, aiming to prioritize the maintenance of the patient's immune system [15]. By enforcing a minimum threshold, we ensure that CD4$^+$ T-cell levels remain within a healthy range throughout the 1500-day treatment horizon, preventing the immune system from dropping to dangerously low levels.

Consequently, the complete *multi-objective binary optimal control problem* is formulated as follows:

$$\begin{aligned}
&\min_{\eta\in\mathcal{E}} && (I_1(\eta),\, I_2(\eta),\, I_3(\eta)) \\
&\text{subject to:} \\
&&& \dot{x}(t) = \lambda - d\,x(t) - r(t)\,x(t)\,v(t), \\
&&& \dot{y}(t) = r(t)\,x(t)\,v(t) - a\,y(t) - p\,y(t)\,z(t), \\
&&& \dot{w}(t) = c\,x(t)\,y(t)\,w(t) - c\,q\,y(t)\,w(t) - b\,w(t), \\
&&& \dot{z}(t) = c\,q\,y(t)\,w(t) - h\,z(t), \\
&&& \dot{v}(t) = k\big(1 - u_P\,\eta_P(t)\big)\,y(t) - \tau\,v(t), \\
&&& \dot{r}(t) = r_0 - u_R\,\eta_R(t), \\
&&& x(t) \geq 500, \quad \forall\, t \in [t_0,\, t_f], \\
&&& \eta_P(t),\, \eta_R(t) \in \{0, 1\}, \quad \forall\, t \in [t_0,\, t_f], \\
&&& x(t_0) = x(0), \quad y(t_0) = y(0), \quad w(t_0) = w(0), \\
&&& z(t_0) = z(0), \quad v(t_0) = v(0), \quad r(t_0) = r(0).
\end{aligned} \tag{9}$$

3.3 Pareto Optimality

Definition. A control strategy $\eta^* \in \mathcal{E}$ is said to be Pareto optimal if there is no other admissible control $\eta \in \mathcal{E}$ such that:

$$I_i(\eta) \leq I_i(\eta^*), \quad \text{for all } i = 1, 2, 3, \tag{10}$$

$$I_i(\eta) < I_i(\eta^*), \quad \text{for at least one } i \in \{1, 2, 3\}. \tag{11}$$

The set of such non-dominated solutions forms the Pareto front, which visualizes the trade-offs between competing treatment goals.

The high-dimensional binary control space considered in this study (e.g., 60 variables per block for two medications over 30 days) leads to significant computational challenges. Due to the exponential growth of the search space, exact solution methods become computationally intractable [3, 6, 7, 8]

In this study, we approximate the Pareto front using NSBGA-II, a binary variant of NSGA-II [5], following the implementation framework in [17]. A comparison of the optimization problem formulations is provided in Table 2 to illustrate the expanded scope of this work. Here, NSBGA-II is applied to determine daily treatment decisions within 30-day simulation blocks. The rationale for this choice is discussed in Section 3.5.

Table 2: Comparison of the optimization frameworks between the proposed work and [17].

Aspect	**Our manuscript**	**Ref. [17]**
Model dimension	Six-state HIV model (x, y, w, z, v, r)	Three-state HIV model (x, y, v)
Objectives	Three objectives: max $CD4^+$ T-cells, min viral load, min treatment burden	Two objectives: min tracking error, min drug usage
Control structure	Two binary controls (PI and RTI) with asynchronous and synchronous scheduling	Single binary control signal
Optimization horizon	1500 days	1500 days

3.4 Constraint Handling via Additive Penalty

To enforce the safety requirement $x(t) \geq 500$ within the NSBGA-II framework, we apply an additive penalty method. Genetic algorithms are naturally suited for unconstrained optimization, so we introduce a penalty function $P(\eta)$ that increases with the cumulative violation of the constraint:

$$P(\eta) = \beta \sum_{t=t_0}^{t_f} \max(0, 500 - x(t)), \tag{12}$$

where $\beta = 10^8$. The fitness of each individual is then evaluated using the augmented objectives $\tilde{I}_i = I_i + P$. By including this penalty across all three objectives, we ensure that infeasible solutions are Pareto-dominated by feasible ones, while the continuous nature of $P(\eta)$ provides a numerical gradient that steers the population toward the feasible region.

3.5 Justification of the Choice of NSBGA-II

The optimization problem considered in this work is a finite-horizon multi-objective scheduling problem in which each treatment decision is binary. Under asynchronous control, the decision vector consists of two binary dosing sequences, one for each drug class, while under synchronous control a single binary sequence is optimized. Consequently, the search space is discrete and combinatorial rather than continuous.

For this reason, we adopted a binary version of NSGA-II (denoted here by NSBGA-II) as the main optimizer. This choice is motivated by both methodological and practical considerations. First, the binary chromosome representation matches the structure of the treatment schedule directly, without requiring continuous relaxation, thresholding, or repair operators. Second, NSGA-II combines elitism, fast non-dominated sorting, and crowding-distance diversity preservation, which are known to be central ingredients for constructing accurate and well-distributed approximations of Pareto fronts in multi-objective evolutionary optimization [5]. In particular, elitism prevents the loss of high-quality non-dominated schedules, while crowding-distance sorting helps preserve diverse trade-offs among immune preservation, viral suppression, and treatment burden.

To evaluate whether this choice is justified relative to other widely used multi-objective metaheuristics, we compared NSBGA-II against three representative alternatives: SPEA2, MOEA/D, and a binary adaptation of MOPSO (hereafter BMOPSO). SPEA2 is another elitist Pareto-based evolutionary algorithm that uses strength-based fitness assignment, density estimation, and archive truncation [22]. MOEA/D decomposes a multi-objective problem into a set of scalar subproblems and solves them collaboratively through neighborhood interactions [20]. BMOPSO belongs to the family of multi-objective particle swarm methods that use an external archive of non-dominated solutions to guide the swarm [4]. These methods are well established and provide meaningful comparators.

Since exact Pareto sets can be computed for short horizons, we performed a benchmark for $L \in \{5, 7, 10\}$ under both asynchronous and synchronous control, using exhaustive enumeration as ground truth. Under asynchronous control, each decision period admits four possible control combinations, so the exact reference front was obtained by enumerating all 4^L admissible schedules. Under synchronous control, only one binary control is applied at each period, so the exact reference front was obtained by enumerating all 2^L admissible schedules. All heuristics were run with the same population size, the same number of generations, and 20 independent runs. Performance was assessed by coverage with respect to the exact Pareto front, normalized generational distance (GD), normalized inverted generational distance (IGD), Pareto set size, and runtime. Each reported value corresponds to the median over the 20 runs.

The benchmark shows that NSBGA-II provides the best overall compromise for the present problem. Under asynchronous control, NSBGA-II achieved exact recovery of the Pareto front

for $L = 5$ and $L = 7$, and maintained a high median coverage of 0.929 for $L = 10$, while remaining the fastest method in all cases. SPEA2 followed closely in accuracy but required nearly double the computational time. MOEA/D showed significantly lower coverage as the horizon increased, and BMOPSO's performance began to degrade at $L = 7$, dropping to a coverage of 0.476 at $L = 10$. Under synchronous control, NSBGA-II recovered the exact front in all tested horizons ($L = 5, 7, 10$) while consistently recording the lowest runtimes. While SPEA2 and BMOPSO also achieved full coverage for the synchronous case, they were substantially slower than NSBGA-II, whereas MOEA/D remained less reliable, with coverage falling sharply as the horizon length increased

Table 3: Benchmark results under asynchronous control. Reported values are medians over 20 independent runs. For each horizon length L, the exact Pareto front was obtained by exhaustive enumeration of all 4^L admissible schedules. Best runtime in each block is highlighted in bold.

L	Algorithm	Coverage	GD_{norm}	IGD_{norm}	Pareto size	Runtime (s)
5	NSBGA-II	1.000	0.000e+00	0.000e+00	11.0	**5.26**
	SPEA2	1.000	0.000e+00	0.000e+00	11.0	9.51
	MOEA/D	0.818	0.000e+00	2.041e-02	9.0	19.56
	BMOPSO	1.000	0.000e+00	0.000e+00	11.0	8.77
7	NSBGA-II	1.000	0.000e+00	0.000e+00	15.0	**6.47**
	SPEA2	1.000	0.000e+00	0.000e+00	15.0	11.73
	MOEA/D	0.733	5.848e-03	4.453e-02	12.0	23.32
	BMOPSO	0.867	0.000e+00	4.780e-03	14.0	9.50
10	NSBGA-II	0.929	0.000e+00	2.382e-03	20.0	**8.68**
	SPEA2	0.905	0.000e+00	7.143e-03	19.0	15.06
	MOEA/D	0.571	1.040e-02	8.270e-02	14.0	26.76
	BMOPSO	0.476	9.583e-03	4.090e-02	16.0	11.03

4 Numerical Implementation and Results

In this section, we present the implementation details and outcomes of our proposed therapy optimization framework using the binary multi-objective genetic algorithm NSBGA-II. We divide the discussion into two parts: first, we analyze the natural progression of the disease without treatment, and then we evaluate the performance of the optimized treatment strategies under both asynchronous and synchronous control.

Table 4: Benchmark results under synchronous control. Reported values are medians over 20 independent runs. For each horizon length L, the exact Pareto front was obtained by exhaustive enumeration of all 2^L admissible schedules. Best runtime in each block is highlighted in bold.

L	Algorithm	Coverage	GD_{norm}	IGD_{norm}	Pareto size	Runtime (s)
5	NSBGA-II	1.000	0.000e+00	0.000e+00	6.0	**4.71**
	SPEA2	1.000	0.000e+00	0.000e+00	6.0	9.04
	MOEA/D	0.833	0.000e+00	3.554e-02	5.0	15.27
	BMOPSO	1.000	0.000e+00	0.000e+00	6.0	8.78
7	NSBGA-II	1.000	0.000e+00	0.000e+00	8.0	**5.80**
	SPEA2	1.000	0.000e+00	0.000e+00	8.0	10.99
	MOEA/D	0.625	1.286e-02	7.585e-02	6.0	17.76
	BMOPSO	1.000	0.000e+00	0.000e+00	8.0	10.22
10	NSBGA-II	1.000	0.000e+00	0.000e+00	11.0	**7.87**
	SPEA2	1.000	0.000e+00	0.000e+00	11.0	13.72
	MOEA/D	0.409	3.198e-02	1.120e-01	7.0	21.50
	BMOPSO	1.000	0.000e+00	0.000e+00	11.0	12.14

4.1 Open-Loop Dynamics (No Treatment)

The simulation is performed using the fourth-order Runge-Kutta (RK4) method [2], a widely used numerical scheme for approximating solutions to ordinary differential equations with higher-order accuracy. For a general control-dependent system of the form:

$$\dot{X}(t) = f(X(t), \eta(t), t), \tag{13}$$

the RK4 method updates the state from t_n to $t_{n+1} = t_n + \Delta t$ according to the following iterative procedure:

$$\begin{aligned} k_1 &= f(X_n, \eta_n, t_n), \\ k_2 &= f(X_n + \frac{\Delta t}{2} k_1, \eta_n, t_n + \frac{\Delta t}{2}), \\ k_3 &= f(X_n + \frac{\Delta t}{2} k_2, \eta_n, t_n + \frac{\Delta t}{2}), \\ k_4 &= f(X_n + \Delta t k_3, \eta_n, t_n + \Delta t), \\ X_{n+1} &= X_n + \frac{\Delta t}{6}(k_1 + 2k_2 + 2k_3 + k_4), \end{aligned} \tag{14}$$

where Δt denotes the time discretization step and X_n represents the state at time t_n. In the present study, this scheme is used to simulate the nonlinear within-host HIV dynamics under the prescribed treatment controls, ensuring numerical stability and precision over the simulation horizon.

To gain a deeper understanding of the natural progression of HIV infection without external intervention, we perform an open-loop simulation, meaning no treatment is applied throughout the simulation horizon: $\eta_P(t) = \eta_R(t) = 0$. This setup isolates the disease's intrinsic dynamics, allowing us to observe how the immune system responds to viral proliferation in the absence of therapy.

The initial state of the system is defined as:

$$X(0) = \left(1000, 0, 10^{-3}, 10^{-7}, 10^{4}, 4 \times 10^{-7}\right),$$

which corresponds to a patient with a strong immune baseline, no prior infection, and a small initial viral and immune activity level.

The resulting trajectories are visualized in Figure 1, which illustrates the temporal evolution of all six state variables under this untreated scenario.

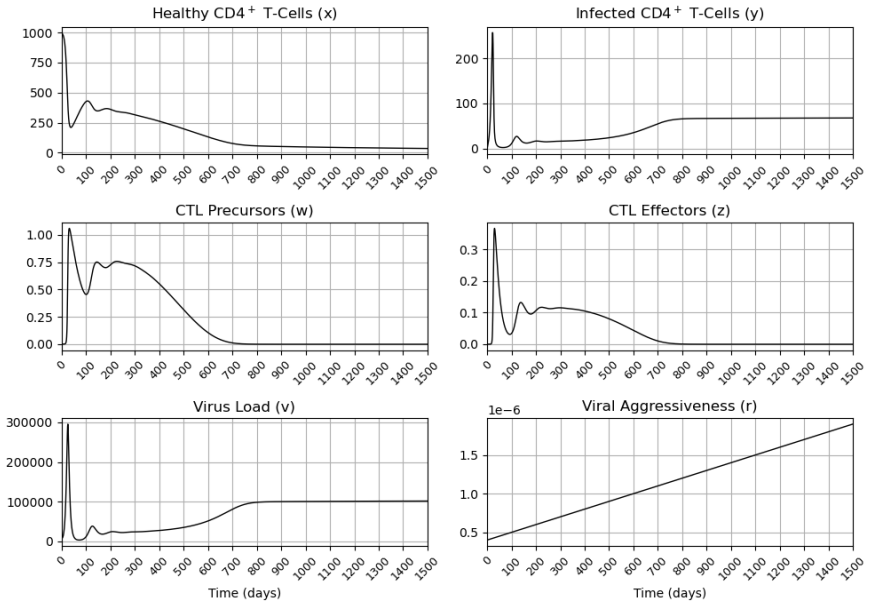

Figure 1: Open-loop response showing disease progression without treatment intervention.

4.2 Closed-Loop Control Strategies with NSBGA-II

The treatment optimization process is based on a block-wise NSBGA-II strategy, where each block spans 30 days. This structure emulates a clinical setting in which the patient's health is monitored periodically, consistent with routine clinical reassessment intervals. In our implementation, the measured state at the end of each block is approximated using simulated state trajectories and then used as the initial condition for the next block. While this differs from

real-world clinical observation, it preserves the principle of adaptive, receding-horizon control.

We evaluate two control strategies:

4.2.1 Strategy 1: Asynchronous Control

Following the open-loop simulation, we observe that CD4$^+$ T-cell levels decline steadily in the absence of treatment, crossing the clinical threshold of 350 cells/μL on day 27. This marks the initiation of antiretroviral therapy in the closed-loop setting. From this point onward, the 1500-day treatment horizon is partitioned into consecutive 30-day blocks, starting precisely at day 27. This yields a total of 49 full treatment blocks, covering 1470 days, followed by 3 leftover days at the end of the horizon. The treatment scheduling is thus aligned with the onset of immune suppression while ensuring full coverage of the simulation period.

In this control strategy, the administration schedules of the two medications, protease inhibitor (PI) and reverse transcriptase inhibitor (RTI), are optimized independently. This results in a 60-dimensional binary control vector per block, with 30 entries for each drug. Each entry represents a daily on/off decision (1 for drug administration, 0 for no administration). The Non-dominated Sorting Binary Genetic Algorithm II (NSBGA-II) is employed to determine Pareto-optimal control strategies for each block by simultaneously minimizing the three conflicting objectives defined in Equations (5)–(7). The resulting Pareto front provides a set of non-dominated trade-offs, allowing a clinician to select a specific strategy based on the patient's priorities. For instance, a clinician might prioritize aggressive immune preservation (min I_1) or, conversely, a reduced treatment burden (min I_3). Accordingly, the framework remains flexible to different clinical selection criteria.

The optimization framework also explicitly accounts for the 3 leftover days that fall outside the final full block. These days are treated as a separate decision segment to ensure that the entire post-treatment-initiation horizon, from day 27 to day 1500, is optimally covered without any temporal gaps.

The complete optimization procedure for Strategy 1 is presented in Algorithm 1.

Figure 2 displays the Pareto fronts for a representative 30-day block, Block 15 (days 447–477), under asynchronous control. Each point corresponds to a non-dominated treatment strategy that reflects a unique trade-off among the three competing objectives. The graph on the left represents the results of selecting the solution that maximizes healthy CD4$^+$ T cells (min I_1) from each previous block, with the current selection highlighted by a blue marker. In contrast, the graph on the right represents the results of selecting the solution that minimizes treatment burden (min I_3) from each previous block, with the current selection highlighted by a green

Algorithm 1 Block-Wise Optimization Under Asynchronous Control

Require: Model parameters; $X(0) = (1000, 0, 10^{-3}, 10^{-7}, 10^{4}, 4 \times 10^{-7})$; $T_{\text{total}} = 1500$ days; $B = 30$ days; $x_{\text{threshold}} = 350$ cells/μL; $x_{\text{safe}} = 500$ cells/μL; $\mathbb{E} = \{0,1\}^{2B}$.

Ensure: Policy $\{(\eta^*_{P,i}, \eta^*_{R,i})\}$; state trajectories over $[0, T_{\text{total}}]$; Pareto fronts $\{\mathcal{F}_i\}$.

1. **Pre-treatment simulation.** Set $\eta_P(t) = \eta_R(t) = 0$ for all t. Compute $t_{\text{start}} \leftarrow \min\{t : x(t) \leq x_{\text{threshold}}\}$ and set $X_1(0) \leftarrow X(t_{\text{start}})$.
2. **Block decomposition.** Compute $N_{\text{blocks}} \leftarrow \lfloor (T_{\text{total}} - t_{\text{start}})/B \rfloor$, $L \leftarrow (T_{\text{total}} - t_{\text{start}}) \bmod B$. Initialize `All_Pareto` $\leftarrow \emptyset$, `Chosen` $\leftarrow \emptyset$.
3. **For** $i = 1$ **to** N_{blocks}:
   a. *Optimization.* Apply NSGA-II over $(\eta_P, \eta_R) \in \{0,1\}^{2B}$ from $X_i(0)$, minimizing augmented objectives ($k = 1, \ldots, B$):

$$P(\eta) = \beta \sum_{k=1}^{B} \max(0, x_{\text{safe}} - x_i(k)), \quad \tilde{I}_j(\eta) = I_j(\eta) + P(\eta),\ j = 1, 2, 3,$$

$$I_1 = -\sum_{k=1}^{B} x_i(k), \quad I_2 = \sum_{k=1}^{B} v_i(k), \quad I_3 = \sum_{k=1}^{B} (\eta_{P,i}(k) + \eta_{R,i}(k)).$$

   b. *Pareto extraction.* Extract Pareto front $\mathcal{F}_i$.
   c. *Schedule selection.* Select $(\eta^*_{P,i}, \eta^*_{R,i}) \in \mathcal{F}_i$ by clinical priority.
   d. *State propagation.* Simulate under $(\eta^*_{P,i}, \eta^*_{R,i})$; update $X_{i+1}(0) \leftarrow X_i(B)$.
   e. *Record.* Append $\mathcal{F}_i$ to `All_Pareto` and $(\eta^*_{P,i}, \eta^*_{R,i})$ to `Chosen`.
4. **Residual block** (only if $L > 0$):
   a. Set $X_{N_{\text{blocks}}+1}(0) \leftarrow X_{N_{\text{blocks}}}(B)$.
   b. Apply NSGA-II over $(\eta_P, \eta_R) \in \{0,1\}^{2L}$ from $X_{N_{\text{blocks}}+1}(0)$.
   c. Extract $\mathcal{F}_{N_{\text{blocks}}+1}$ and select optimal schedule $(\eta^*_{P,N_{\text{blocks}}+1}, \eta^*_{R,N_{\text{blocks}}+1})$ by clinical priority.
   d. Simulate and append results to `All_Pareto` and `Chosen`.
5. **Return** `Chosen`, full state trajectories, and `All_Pareto`.

marker. These two distinct visualizations highlight how the available trade-offs evolve based on the prioritized objective.

Figure 3 illustrates the closed-loop trajectories and corresponding treatment schedules under asynchronous control. We present results based on the Pareto-optimal solution from each block that minimizes the first objective function (Best I_1, blue trajectory) and the third objective function (Best I_3, green trajectory).

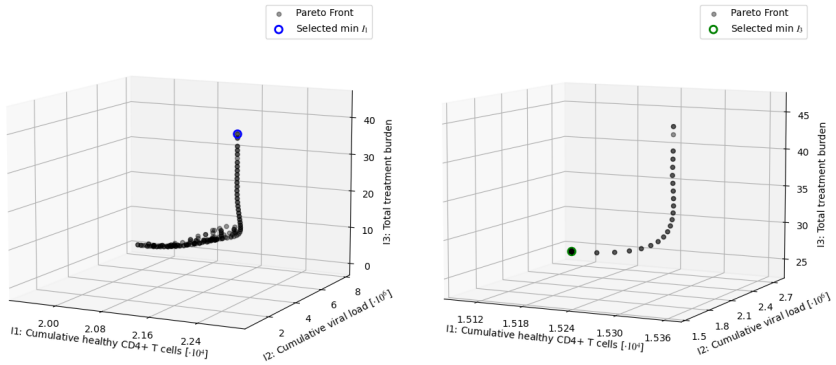

Figure 2: Pareto fronts under asynchronous control.

4.2.2 Strategy 2: Synchronous Control

As in Strategy 1, treatment begins on day 27, immediately after $CD4^+$ T-cell levels fall below the clinical threshold of 350 cells/μL in the open-loop scenario. The 1500-day horizon is thus divided into 49 full 30-day blocks and 3 leftover days, ensuring a consistent temporal structure across both control strategies.

In this control strategy, both PI and RTI are administered synchronously, i.e., $\eta_P(t) = \eta_R(t) = \eta(t)$, resulting in a single 30-dimensional binary decision vector per block. This simplification reduces the dimensionality of the decision space and may facilitate improved patient adherence by unifying drug schedules.

The optimization in this setting considers three objectives: maximizing healthy $CD4^+$ T-cell levels, minimizing viral load, and reducing the cumulative treatment burden, here measured through the shared binary control $\eta(t)$. Accordingly, the third objective is defined as

$$I_3(\eta) = \sum_{t=t_0}^{t_f} \eta(t) \tag{15}$$

The complete optimization procedure for Strategy 2 is presented in Algorithm 2.

Figure 4 displays the Pareto fronts for a representative 30-day block, Block 15 (days 447–477), under synchronous control. Each point corresponds to a non-dominated treatment strategy

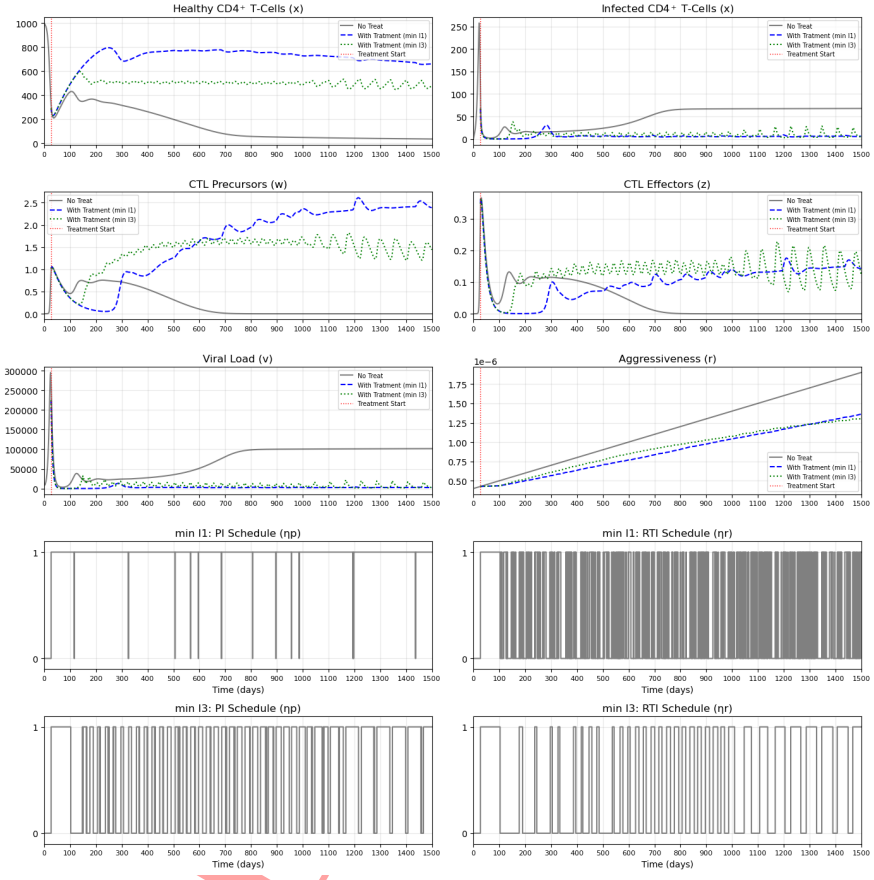

Figure 3: Optimized closed-loop response under asynchronous control.

that reflects a unique trade-off among the three competing objectives. The graph on the left represents the results of selecting the solution that maximizes healthy CD4$^+$ T cells (min I_1) from each previous block, with the current selection highlighted by a blue marker. In contrast, the graph on the right represents the results of selecting the solution that minimizes treatment burden (min I_3) from each previous block, with the current selection highlighted by a green marker. These two distinct visualizations highlight how the available trade-offs evolve based on the prioritized objective.

Figure 5 illustrates the closed-loop trajectories and corresponding treatment schedules under synchronous control. We present results based on the Pareto-optimal solution from each block that minimizes the first objective function (min I_1, blue trajectory) and the third objective function (min I_3, green trajectory).

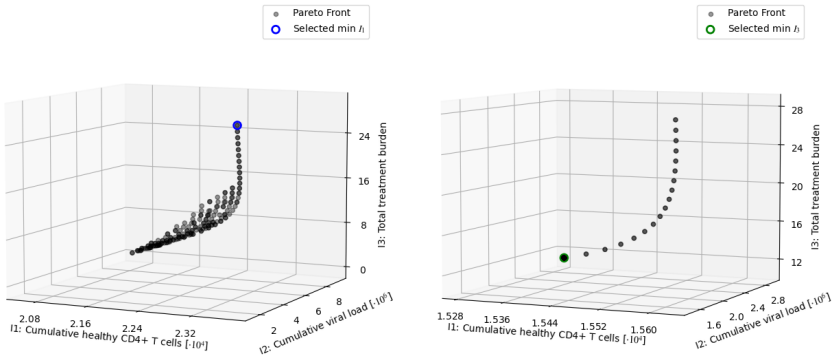

Figure 4: Pareto fronts under synchronous control.

The optimization experiments were conducted on a system with an Intel Core i5-8265U processor (4 cores, 1.6 GHz) and 8 GB of RAM. The average runtime per block was 22.78s for asynchronous control and 21.96s for synchronous control.

4.3 Descriptive Analysis of the Selected Optimized Schedules

To interpret the treatment structures generated by the optimization procedure, a descriptive analysis was performed on the selected binary schedules for both the min I_1 and min I_3 solutions. In this analysis, a pulse denotes a consecutive interval of active treatment, while a rest period denotes an interval of inactivity. Accordingly, pulse and rest lengths quantify the durations of therapeutic phases and drug-free windows, respectively.

Under asynchronous control, the two solutions exhibit markedly different temporal organizations. The min I_1 schedule is characterized by a nearly continuous treatment backbone, with the protease inhibitor (PI) active during 98.9% of the window and very long pulses (mean of

Algorithm 2 Block-Wise Optimization Under Synchronous Control

Require: Model parameters; $X(0) = (1000, 0, 10^{-3}, 10^{-7}, 10^{4}, 4 \times 10^{-7})$; $T_{\text{total}} = 1500$ days; $B = 30$ days; $x_{\text{threshold}} = 350$ cells/μL; $x_{\text{safe}} = 500$ cells/μL; $\mathbb{E} = \{0,1\}^B$.

Ensure: Policy $\{\eta_i^*\}$; state trajectories over $[0, T_{\text{total}}]$; Pareto fronts $\{\mathcal{F}_i\}$.

1. **Pre-treatment simulation.** Set $\eta(t) = 0$ for all t. Compute $t_{\text{start}} \leftarrow \min\{t : x(t) \leq x_{\text{threshold}}\}$ and set $X_1(0) \leftarrow X(t_{\text{start}})$.
2. **Block decomposition.** Compute $N_{\text{blocks}} \leftarrow \lfloor (T_{\text{total}} - t_{\text{start}})/B \rfloor$, $L \leftarrow (T_{\text{total}} - t_{\text{start}}) \bmod B$. Initialize `All_Pareto` $\leftarrow \emptyset$, `Chosen` $\leftarrow \emptyset$.
3. **For** $i = 1$ **to** N_{blocks}:
   a. *Optimization.* Apply NSGA-II over $\eta \in \{0,1\}^B$ from $X_i(0)$, minimizing augmented objectives ($k = 1, \ldots, B$):

$$P(\eta) = \beta \sum_{k=1}^{B} \max(0, x_{\text{safe}} - x_i(k)), \quad \tilde{I}_j(\eta) = I_j(\eta) + P(\eta),\ j = 1, 2, 3,$$

$$I_1 = -\sum_{k=1}^{B} x_i(k), \quad I_2 = \sum_{k=1}^{B} v_i(k), \quad I_3 = \sum_{k=1}^{B} \eta_i(k).$$

   b. *Pareto extraction.* Extract Pareto front $\mathcal{F}_i$.
   c. *Schedule selection.* Select $\eta_i^* \in \mathcal{F}_i$ by clinical priority.
   d. *State propagation.* Simulate under η_i^*; update $X_{i+1}(0) \leftarrow X_i(B)$.
   e. *Record.* Append $\mathcal{F}_i$ to `All_Pareto` and η_i^* to `Chosen`.
4. **Residual block** (only if $L > 0$):
   a. Set $X_{N_{\text{blocks}}+1}(0) \leftarrow X_{N_{\text{blocks}}}(B)$.
   b. Apply NSGA-II over $\eta \in \{0,1\}^L$ from $X_{N_{\text{blocks}}+1}(0)$.
   c. Extract $\mathcal{F}_{N_{\text{blocks}}+1}$ and select $\eta^*_{N_{\text{blocks}}+1}$ by clinical priority.
   d. Simulate and append results to `All_Pareto` and `Chosen`.
5. **Return** `Chosen`, full state trajectories, and `All_Pareto`.

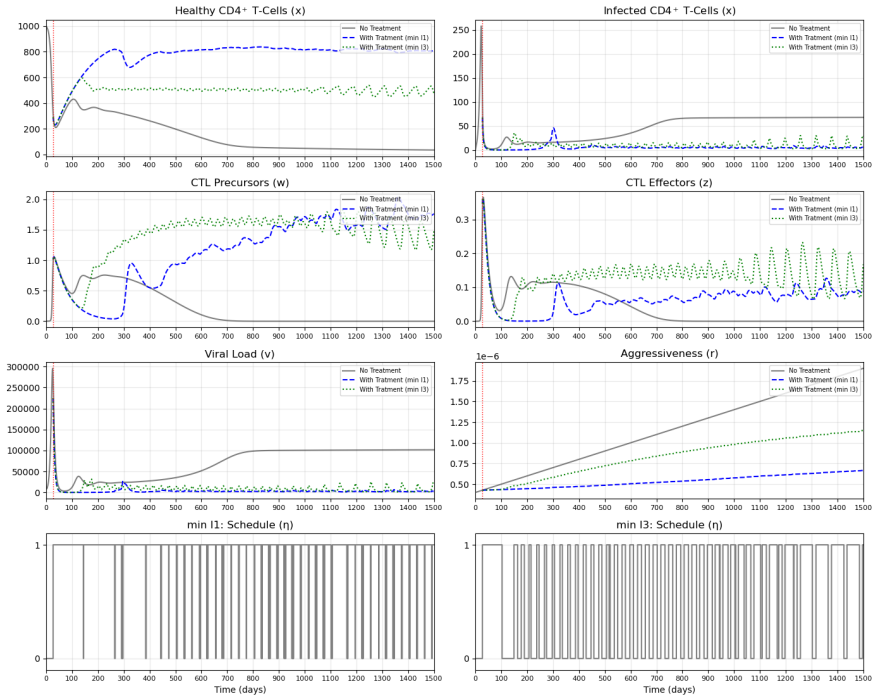

Figure 5: Optimized closed-loop response under synchronous control.

104.14 days). Conversely, the min I_3 solution produces a more intermittent structure where the PI is active only 62.7% of the time, with shorter pulses (mean of 14.44 days) and significantly longer rest periods (mean of 8.71 days). While the min I_1 joint schedule avoids global treatment interruptions (max rest of 2 days), the min I_3 solution allows for extended joint rest periods of up to 45 days, reflecting a strategy that prioritizes drug reduction.

Under synchronous control, both solutions maintain a structured pulse pattern, though the intensity differs. The min I_1 synchronous schedule is predominantly sustained (93.1% ON fraction), with short interruptions. In contrast, the min I_3 synchronous schedule reduces the ON fraction to 56.7%, increasing the mean rest period from 1.6 to 13.9 days and allowing a maximum rest of 46 days. This indicates that as the optimization goal shifts from I_1 toward I_3, the resulting schedules transition from a *sustained coverage* pattern to a *structured pulsing* approach that incorporates substantial drug-free intervals.

Overall, the selected schedules display clear temporal structures rather than irregular patterns. The main difference lies in the density of the pulses: min I_1 results in a high-density, nearly continuous treatment, whereas min I_3 leverages the system dynamics to allow for significant rest periods without losing control over the viral dynamics.

All statistics are computed over the 1473 post-initiation days (days 27–1500).

Table 5: Descriptive statistics of the selected optimized schedules (min I_1 vs. min I_3). [2]

Solution	Control	Schedule	ON days	ON fraction	No. of switches	No. of pulses	No. of rests	Mean pulse	Max pulse	Mean rest	Max rest
min I_1	Asynch.	PI	1458	0.989	26	14	13	104.14	239	1.15	2
	Asynch.	RTI	601	0.408	506	254	253	2.37	76	3.45	19
	Asynch.	Any treatment active	1459	0.990	24	13	12	112.23	303	1.17	2
	Synch.	Common schedule	1372	0.931	124	63	62	21.80	120	1.60	5
min I_3	Asynch.	PI	924	0.627	126	64	63	14.44	76	8.71	45
	Asynch.	RTI	666	0.452	64	33	32	20.18	76	25.22	74
	Asynch.	Any treatment active	924	0.627	126	64	63	14.44	76	8.71	45
	Synch.	Common schedule	835	0.567	92	47	46	17.80	76	13.90	46

5 Sensitivity and Robustness Analysis

In addition to the nominal simulations presented above, we conducted supplementary analyses to evaluate the robustness of the proposed framework with respect to parameter uncertainty and its sensitivity to the choice of block length.

5.1 Parametric Sensitivity and Robustness Analysis

To examine the effect of parameter uncertainty, a one-at-a-time parametric sensitivity analysis was performed around the nominal parameter set [18]. The parameters r_0, k, and λ were selected because they differ from one patient to another [13]. The parameters k and λ were perturbed by $\pm 10\%$, whereas r_0 was perturbed by $\pm 5\%$. A smaller perturbation range was adopted for r_1 because larger negative variations produced biologically infeasible trajectories.

For all subsequent analyses, the specific solution selected from the Pareto front for evaluation is the one that maximizes the cumulative healthy $CD4^+$ T cell count.

Two complementary levels of analysis were considered. In the first level, the treatment schedule computed for the nominal parameter set was kept fixed, and only the parameter under study was perturbed. The system was then re-simulated using this same schedule. This level evaluates the robustness of the nominally designed therapy, that is, whether the original treatment remains effective when the true parameter values differ moderately from their nominal estimates.

In the second level, after perturbing one parameter, the multi-objective optimization procedure was performed again for the perturbed model. A new treatment schedule was therefore

computed for each perturbed case. This level evaluates the sensitivity of the optimal design itself by showing how the resulting trajectories, cumulative outcomes, and treatment patterns change when the parameter values are modified.

Both levels of analysis were carried out under asynchronous and synchronous control. The results are presented through the trajectories of healthy $CD4^+$ T cells, together with the cumulative healthy $CD4^+$ cells, cumulative viral load, and cumulative treatment effort. For clarity of presentation, the first quantity is reported as the positive cumulative healthy $CD4^+$ count, although in the optimization procedure it is implemented through the minimization of its negative value.

5.1.1 Level 1: robustness of the nominally designed schedule.

Tables 6 and 7, together with Fig. 6, show the effect of parameter perturbations when the nominal treatment schedule is kept unchanged. Under both control strategies, decreasing r_0 by 5% slightly improves the outcomes, whereas increasing r_0 by 5% slightly worsens them. More precisely, under asynchronous control, the cumulative healthy $CD4^+$ cells increase by 1.27% and the cumulative viral load decreases by 1.15% for the negative perturbation. This indicates that the model is only mildly sensitive to moderate changes in r_0.

The parameter k has a stronger influence, particularly on the cumulative viral load. Under asynchronous control, a decrease of 10% in k increases the cumulative healthy $CD4^+$ cells by 2.78% and reduces the cumulative viral load by 9.20%, whereas a 10% increase in k decreases the $CD4^+$ count by 3.08% and raises the viral load by 11.04%. A similar pattern is observed under synchronous control, with variations of approximately $+2.40\%$ and -11.80% for $k-10\%$, and -1.93% and $+9.69\%$ for $k+10\%$. These results confirm that viral production is a significant source of sensitivity.

Among the three perturbed parameters, λ produces the largest changes. Under asynchronous control, a decrease of 10% in λ reduces the cumulative healthy $CD4^+$ cells by 13.65% and increases the cumulative viral load by 14.30%, while a positive perturbation improves the $CD4^+$ count by 13.18%. Under synchronous control, the corresponding changes are -11.48% and $+8.30\%$ for $\lambda-10\%$, and $+11.91\%$ and -8.56% for $\lambda+10\%$. Therefore, λ is the most influential parameter among those considered in this level.

It is also worth noting that the cumulative treatment effort remains unchanged at this first level of analysis under both control strategies (2059 for asynchronous and 1372 for synchronous). This is expected, since the treatment schedule is fixed. Overall, the same qualitative trends are observed under both control strategies, though synchronous control appears slightly more robust to perturbations in λ.

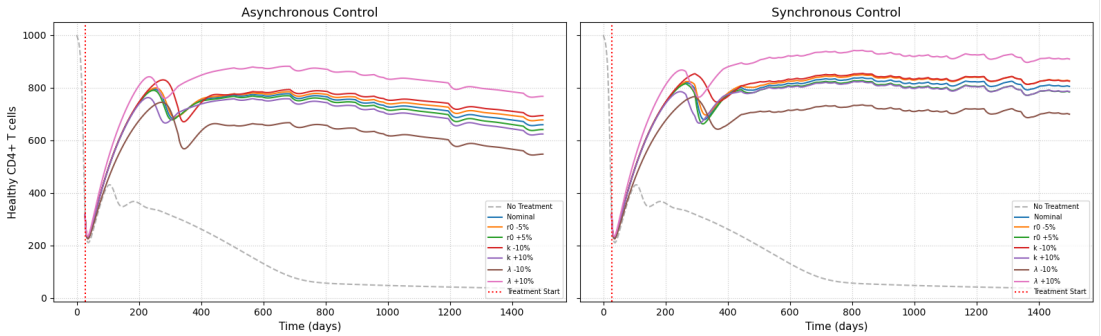

Figure 6: Level 1 sensitivity analysis: full-horizon trajectories of healthy CD4$^+$ T cells under parameter perturbations for asynchronous and synchronous control.

Table 6: Level 1 sensitivity analysis under asynchronous control.

Perturbation	Cumulative healthy CD4$^+$ cells	Cumulative viral load	Cumulative treatment effort
Nominal	1041385.8040	5211596.1507	2059.0000
$r_0 - 5\%$	1054648.6397 (+1.27%)	5151877.4853 (-1.15%)	2059.0000 (+0.00%)
$r_0 + 5\%$	1028095.8635 (-1.28%)	5273382.7117 (+1.19%)	2059.0000 (+0.00%)
$k - 10\%$	1070353.7038 (+2.78%)	4731947.3171 (-9.20%)	2059.0000 (+0.00%)
$k + 10\%$	1009355.8939 (-3.08%)	5786720.2218 (+11.04%)	2059.0000 (+0.00%)
$\lambda - 10\%$	899244.2409 (-13.65%)	5956710.5004 (+14.30%)	2059.0000 (+0.00%)
$\lambda + 10\%$	1178631.4079 (+13.18%)	4736738.7474 (-9.11%)	2059.0000 (+0.00%)

Table 7: Level 1 sensitivity analysis under synchronous control.

Perturbation	Cumulative healthy CD4$^+$ cells	Cumulative viral load	Cumulative treatment effort
Nominal	1136262.5643	5310730.4863	1372.0000
$r_0 - 5\%$	1153198.8809 (+1.49%)	5199428.3025 (-2.10%)	1372.0000 (+0.00%)
$r_0 + 5\%$	1119507.6226 (-1.47%)	5416923.1698 (+2.00%)	1372.0000 (+0.00%)
$k - 10\%$	1163563.4268 (+2.40%)	4683949.1315 (-11.80%)	1372.0000 (+0.00%)
$k + 10\%$	1114327.1659 (-1.93%)	5825392.6307 (+9.69%)	1372.0000 (+0.00%)
$\lambda - 10\%$	1005805.1864 (-11.48%)	5751512.0606 (+8.30%)	1372.0000 (+0.00%)
$\lambda + 10\%$	1271628.9677 (+11.91%)	4856346.3957 (-8.56%)	1372.0000 (+0.00%)

5.1.2 Level 2: sensitivity with re-optimization.

Tables 8 and 9, together with Fig. 7, report the results obtained when the optimization is repeated for each perturbed parameter set. In this case, the treatment schedule adapts, and the cumulative effort varies.

For r_0, the re-optimized solutions show improvements in CD4$^+$ counts of 1.58% and 1.97% for $r_0 - 5\%$ under asynchronous and synchronous control, respectively. Interestingly, the optimization compensates for these changes by slightly increasing treatment effort (up to $+0.73\%$).

For k, the effect of re-optimization is more pronounced than in Level 1. Under asynchronous control, $k-10\%$ allows for a 3.70% increase in CD4$^+$ cells and a significant 16.53% reduction in viral load, even with 1.31% less treatment effort. Conversely, $k + 10\%$ results in a 19.24% increase in viral load despite the optimized adaptation. This highlights k as a critical driver of the viral burden.

The parameter λ remains the dominant sensitivity factor. Under asynchronous control, $\lambda - 10\%$ leads to an 11.70% reduction in cumulative healthy CD4$^+$ cells and a 14.11% increase in viral load, requiring a significant 4.95% increase in treatment effort to maintain stability. Under synchronous control, $\lambda + 10\%$ improves outcomes by 12.08% in CD4$^+$ count and reduces viral load by 10.67%.

Unlike Level 1, the adaptation of the treatment schedule shows that for parameters that "worsen" the disease state (like decreasing λ or increasing r_0), the optimizer generally increases the treatment effort to mitigate the damage. For parameters that "improve" the disease state (like increasing λ), the optimizer often finds more efficient schedules with slightly lower drug usage.

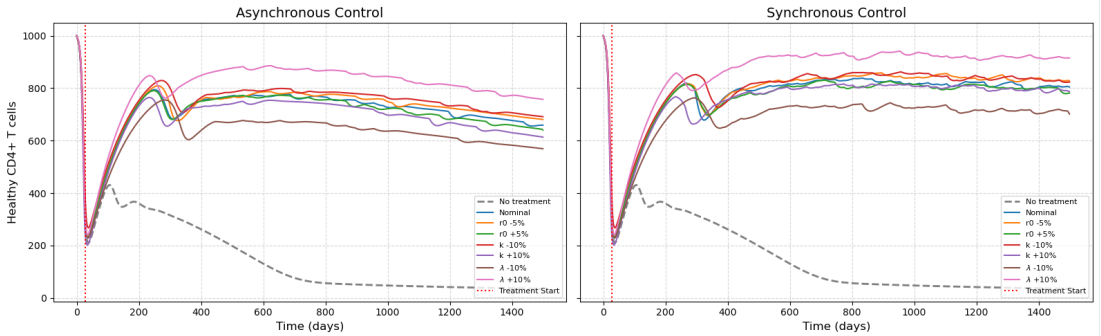

Figure 7: Level 2 sensitivity analysis: full-horizon trajectories of healthy CD4$^+$ T cells under parameter perturbations with re-optimization for asynchronous and synchronous control.

Table 8: Level 2 sensitivity analysis under asynchronous control.

Perturbation	**Cumulative healthy CD4$^+$ cells**	**Cumulative viral load**	**Cumulative treatment effort**
Nominal	1041385.8040	5211596.1507	2059.0000
$r_0 - 5\%$	1057811.6070 (+1.58%)	5176089.0624 (-0.68%)	2063.0000 (+0.19%)
$r_0 + 5\%$	1029614.6395 (-1.13%)	5263327.1711 (+0.99%)	2074.0000 (+0.73%)
$k - 10\%$	1079869.0308 (+3.70%)	4350233.8205 (-16.53%)	2032.0000 (-1.31%)
$k + 10\%$	1000130.6810 (-3.96%)	6214433.9974 (+19.24%)	2026.0000 (-1.60%)
$\lambda - 10\%$	919507.2520 (-11.70%)	5946997.9717 (+14.11%)	2161.0000 (+4.95%)
$\lambda + 10\%$	1178298.3171 (+13.15%)	4689409.3826 (-10.02%)	2004.0000 (-2.67%)

Table 9: Level 2 sensitivity analysis under synchronous control.

Perturbation	Cumulative healthy CD4$^+$ cells	Cumulative viral load	Cumulative treatment effort
Nominal	1136262.5643	5310730.4863	1372.0000
$r_0 - 5\%$	1158629.8836 (+1.97%)	5126116.7283 (-3.48%)	1382.0000 (+0.73%)
$r_0 + 5\%$	1123020.8040 (-1.17%)	5314702.5687 (+0.07%)	1377.0000 (+0.36%)
$k - 10\%$	1171808.0806 (+3.13%)	4350223.3130 (-18.09%)	1386.0000 (+1.02%)
$k + 10\%$	1110208.2508 (-2.29%)	6222343.5786 (+17.17%)	1372.0000 (+0.00%)
$\lambda - 10\%$	1014441.2054 (-10.72%)	5819595.9589 (+9.58%)	1388.0000 (+1.17%)
$\lambda + 10\%$	1273499.5607 (+12.08%)	4744076.6721 (-10.67%)	1371.0000 (-0.07%)

Comparative Discussion. The two levels of analysis provide complementary information. Level 1 demonstrates that the nominally designed therapy is robust, maintaining qualitative effectiveness even without adaptation. Level 2 evaluates how the optimal treatment strategy adapts to patient-specific variations. In both levels, the results are consistent: decreasing r_0 or k improves outcomes, while increasing them worsens results. The parameter λ is consistently the most influential factor. Furthermore, synchronous control demonstrates a slightly better robustness profile, particularly regarding the sensitivity of the viral load to variations in λ. Overall, these results indicate that the proposed control framework is reliable under moderate parametric uncertainty.

5.2 Block-Size Sensitivity Analysis

To examine the influence of the block length on the obtained treatment strategies, an additional sensitivity analysis was carried out by repeating the block-wise optimization with block sizes of 15, 30, and 60 days. For comparison, we also considered the case where the whole remaining treatment horizon was optimized at once. The same selection rule as in the main study was retained, namely choosing from each Pareto set the solution that maximises the cumulative amount of healthy CD4$^+$ T cells.

The resulting CD4$^+$ T-cell trajectories for asynchronous and synchronous control are displayed in Figure 8. In all tested cases, the optimized treatment strategies led to a substantial improvement over the no-treatment scenario. However, clear differences appear when the block length is varied.

Under asynchronous control, shorter blocks produced better preservation of healthy $CD4^+$ T cells over the treatment horizon. In particular, the 15-day block size gave the best result, with a cumulative healthy-cell value of 1,120,494.319, followed by the 30-day block size with 1,041,385.804, whereas the 60-day block size yielded a lower value of 962,891.686. The same tendency can be observed in Figure 8, where the 15-day strategy maintains the highest $CD4^+$ T-cell trajectory for most of the treatment interval. This improvement is accompanied by a larger treatment effort, since the cumulative treatment amount increased from 1735 for 60-day blocks to 2059 for 30-day blocks and 2516 for 15-day blocks. Thus, under asynchronous control, decreasing the block length improves health outcomes, but at the price of more frequent treatment activation.

Under synchronous control, a similar trend was observed where decreasing the block size led to progressively better health outcomes. The 15-day block size provided the best overall performance, with the highest cumulative healthy-cell value, equal to 1,181,151.700, and the lowest cumulative viral load, equal to 4,547,773.644. The 30-day block size followed with 1,136,262.564 cumulative healthy cells and 5,310,730.486 cumulative viral load, whereas the 60-day block size showed a more visible deterioration, with 1,101,169.224 cumulative healthy cells and 5,843,341.825 cumulative viral load. Figure 8 confirms that the trajectories for 15-day and 30-day strategies remain superior to the 60-day strategy, which preserves fewer $CD4^+$ T cells over time.

The global-horizon optimization produced significantly weaker results under both control strategies. In the asynchronous case, it led to the lowest cumulative healthy-cell value, 824,369.092, together with a much higher cumulative viral load of 11,185,704.536. Similarly, in the synchronous case, it produced 867,693.499 cumulative healthy cells and 10,204,355.022 cumulative viral load, which are both substantially less favorable than the corresponding block-wise results. This behavior can also be observed in Figure 8, where the global strategy remains well below the block-wise trajectories under both control strategies.

Overall, these results show that the conclusions of the study remain qualitatively stable when the block size is varied. Under both asynchronous and synchronous control, shorter blocks are more beneficial in terms of preserving healthy cells and reducing viral burden, although they require a larger treatment amount. While the 15-day block size provides the best biological results, the choice of 30-day blocks remains well-justified as it yields strong performance while remaining consistent with the monthly clinical reassessment motivation adopted in this work.

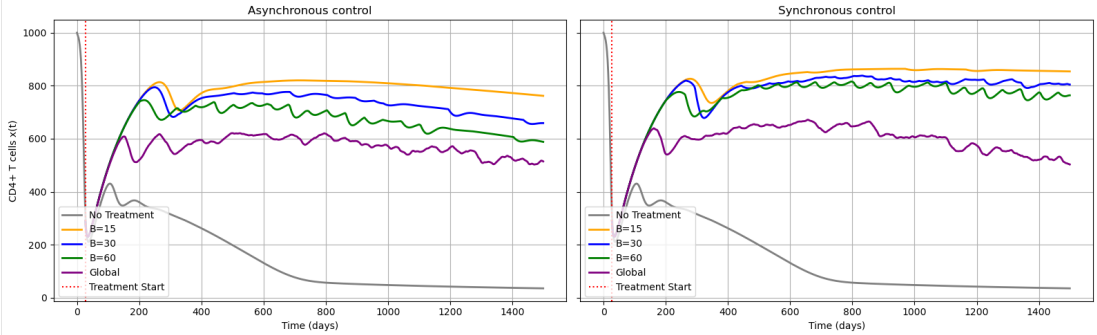

Figure 8: Block-size sensitivity analysis: full-horizon trajectories of healthy $CD4^+$ T cells for asynchronous and synchronous control.

Table 10: Block-size sensitivity analysis under asynchronous control.

Block length (days)	Cum. healthy cells	Cum. virus load	Treatment	Final x	Final v
15-day blocks	1120494.319	4790092.772	2516	761.948	2425.885
30-day blocks	1041385.804	5211596.151	2059	659.007	2700.993
60-day blocks	962891.686	5922411.354	1735	588.216	3299.435
Global horizon	824369.092	11185704.536	1765	514.482	7074.965

Table 11: Block-size sensitivity analysis under synchronous control.

Block length (days)	Cum. healthy cells	Cum. virus load	Treatment	Final x	Final v
15-day blocks	1181151.700	4547773.644	1468	854.151	2112.406
30-day blocks	1136262.564	5310730.486	1372	804.496	2792.933
60-day blocks	1101169.224	5843341.825	1302	763.890	3283.389
Global horizon	867693.499	10204355.022	944	502.866	8616.650

6 Conclusion

Compared with existing multi-objective HIV ART control studies, the present work explicitly enforces binary daily dosing and investigates synchronous and asynchronous PI/RTI scheduling over successive 30-day optimization blocks. The proposed approach was developed on the basis of a six-state HIV dynamical model and solved using NSBGA-II to identify Pareto-optimal treatment schedules that balance immune preservation, viral suppression, and treatment burden. The results demonstrate the ability of the proposed framework to generate clinically meaningful treatment schedules under both asynchronous and synchronous control, while accounting for the trade-offs among the considered objectives. These findings highlight the potential of the proposed framework as a computational decision-support tool for exploring HIV treatment scheduling strategies tailored to patient-specific conditions.

Limitations. The proposed framework is developed under deterministic HIV dynamics and does not explicitly incorporate stochastic variability or measurement noise inherent in clinical settings. Although a sensitivity analysis was performed, additional sources of uncertainty may affect real-world applicability.

Future Work. Future work will build on the present HIV-specific framework by extending the current sensitivity and robustness analysis toward stochastic uncertainty modeling to support more robust and personalized HIV therapy strategies. Extension to other chronic diseases may also be possible, subject to disease-specific reformulation.

Declarations

Availability of Supporting Data

All data generated or analyzed during this study are included in this published paper.

Funding

The author conducted this research without any funding, grants, or support.

Conflict of Interest

The author declares that they have no known competing financial interests or personal relationships that could have influenced the work reported in this paper.

Author Contributions

Islem Bennadja contributed to conceptualization, methodology, formal analysis, software implementation, data curation, writing of the original draft, and preparation of the numerical results. **Omar Kebiri** contributed to supervision, validation, review and editing of the manuscript, and the overall scientific guidance of the study. **Djamal Chaabane** contributed to supervision, validation, review and editing of the manuscript, and the overall scientific guidance of the study. All authors read and approved the final manuscript.

Artificial Intelligence Statement

Artificial intelligence (AI) tools, including large language models, were used solely for language editing and improving readability. AI tools were not used for generating ideas, performing analyses, interpreting results, or writing the scientific content. All scientific conclusions and intellectual contributions were made exclusively by the authors.

Publisher's Note

The publisher remains neutral regarding jurisdictional claims in published maps and institutional affiliations.

References

[1] Ahmed, A., Hill, M., Dong, K.L., Wiseman Ngcobo, M., Zulu, A., Langa, N., Maphalala, L., Pillay, V., MPhil, M.M., Tran, W., Lau, R., Stockman, J.K., Thumbi Ndung'u, I., Karine Dubé, K. (2026). "Stress and coping during an HIV cure-related trial with an analytical treatment interruption: a qualitative assessment of the experiences of young women in Durban, South Africa". *Journal of the International Association of Providers of AIDS Care*, 25, 1–17. https://doi.org/10.1177/23259582261423985

[2] Akinsola, V. (2023). "Numerical methods: Euler and Runge–Kutta". *Qualitative and Computational Aspects of Dynamical Systems*. https://doi.org/10.5772/intechopen.108533

[3] Alweshah, M., Jebril, H., Kassaymeh, S., Almiani, M., Alkhalaileh, S., Rjoub, G. (2026). "Optimizing feature selection in cancer microarray data using a heap-driven evolutionary framework for high-dimensional spaces". *Scientific Reports*, 16, 6726. https://doi.org/10.1038/s41598-026-37803-5

[4] Coello Coello, C.A., Lechuga, M.S. (2002). "MOPSO: A proposal for multiple objective particle swarm optimization". *Proceedings of the 2002 Congress on Evolutionary Computation (CEC'02)*, 2, 1051–1056. https://doi.org/10.1109/CEC.2002.1004388

[5] Deb, K., Pratap, A., Agarwal, S., Meyarivan, T. (2002). "A fast and elitist multiobjective genetic algorithm: NSGA-II". *IEEE Transactions on Evolutionary Computation*, 6(2), 182–197. https://doi.org/10.1109/4235.996017

[6] Ehrgott, M. (2005). *Multicriteria Optimization*. Springer Science & Business Media. https://doi.org/10.1007/3-540-27659-9

[7] Hashemi Borzabadi, A., Hasanabadi, M., Sadjadi, N. (2016). "Approximate Pareto optimal solutions of multi-objective optimal control problems by evolutionary algorithms". *Control and Optimization in Applied Mathematics*, 1(1), 1–19. https://mathco.journals.pnu.ac.ir/article_2033.html

[8] Kantour, N., Bouroubi, S., Chaabane, D. (2018). "A parallel MOEA with criterion-based selection applied to the knapsack problem". *arXiv preprint arXiv:1811.02271*. https://doi.org/10.48550/arXiv.1811.02271

[9] Landi, A., Mazzoldi, A., Andreoni, C., Bianchi, M., Cavallini, A., Laurino, M., Ricotti, L., Iuliano, R., Matteoli, B., Ceccherini-Nelli, L. (2008). "Modelling and control of HIV dynamics". *Computer Methods and Programs in Biomedicine*, 89(2), 162–168. https://doi.org/10.1016/j.cmpb.2007.08.003

[10] Ndung'u, T., Dong, K.L., Colby, D.J., et al. (2026). "Recommendations from the 2nd consensus workshop on analytical treatment interruption in HIV research trials". *The Lancet HIV*, 13(4), e271–e281. https://doi.org/10.1016/S2352-3018(25)00373-X

[11] Nuwagaba, J., Li, J.A., Ngo, B., Sutton, R.E. (2025). "30 years of HIV therapy: Current and future antiviral drug targets". *Virology*, 603, 110362. https://doi.org/10.1016/j.virol.2024.110362

[12] Perelson, A.S., Kirschner, D.E., De Boer, R. (1993). "Dynamics of HIV infection of $CD4^+$ T cells". *Mathematical Biosciences*, 114(1), 81–125. https://doi.org/10.1016/0025-5564(93)90043-A

[13] Rivadeneira, P.S., Moog, C.H., Stan, G.-B., Costanza, V., Brunet, C., Raffi, F., Ferré, V., Mhawej, M.-J., Biafore, F., Ouattara, D.A. (2014). "Mathematical modeling of HIV dynamics after antiretroviral therapy initiation: a clinical research study". *AIDS Research and Human Retroviruses*, 30(9), 831–834. https://doi.org/10.1089/aid.2013.0286

[14] Salami, D., Koech, E., Turan, J.M., Stafford, K.A., Nyagah, L.M., Ohakanu, S., Ngugi, A.K., Charurat, M. (2026). "Prediction of first and multiple antiretroviral therapy interruptions in people living with HIV: Comparative survival analysis using Cox and ex-

plainable machine learning models". *JMIR Medical Informatics*, 14(1), e78964. https://doi.org/10.2196/78964

[15] Saravanan, S., Vignesh, R., Rengarajan, S., Vivekanandan, T., Yong, Y.K., Varsha, V., Mounika, P., Sivamalar, S., Vidya, M., Shankar, E.M., Larsson, M., Velu V., Raju, S., Balakrishnan, P., Nisha, B., Venkateswaran, A.R., Kannan, R. (2026). "Negative influence of age and low baseline CD4 on T helper cell recovery among HIV-infected individuals". *Frontiers in Public Health*, 14, 1729–1745. https://doi.org/10.3389/fpubh.2026.1729238

[16] UNAIDS. (2025). "Global HIV & AIDS statistics — Fact sheet". *Joint United Nations Programme on HIV/AIDS*. https://www.unaids.org/en/resources/fact-sheet

[17] Vafamand, A., Vafamand, N., Zarei, J., Razavi-Far, R., Saif, M. (2021). "Multi-objective NSBGA-II control of HIV therapy with monthly output measurement". *Biomedical Signal Processing and Control*, 68, 102561. https://doi.org/10.1016/j.bspc.2021.102561

[18] Mio Heinrich, M., Rosenblatt, M., Wieland, F.-G., Stigter, H., Timmer, J. (2025). "On structural and practical identifiability: Current status and update of results". *Current Opinion in Systems Biology*, 41, 100546. https://doi.org/10.1016/j.coisb.2025.100546

[19] Wodarz, D., Nowak, M.A. (1999). "Specific therapy regimes could lead to long-term immunological control of HIV". *Proceedings of the National Academy of Sciences*, 96(25), 14464–14469. https://doi.org/10.1073/pnas.96.25.14464

[20] Zhang, Q., Li, H. (2007). "MOEA/D: A multiobjective evolutionary algorithm based on decomposition". *IEEE Transactions on Evolutionary Computation*, 11(6), 712–731. https://doi.org/10.1109/TEVC.2007.892759

[21] Ziani, J.S., Silva, G.P.Z., Monteiro, F.L. (2026). "Factors associated with the interruption of antiretroviral therapy in hospitalized people living with HIV: A multivariate analysis". *The Brazilian Journal of Infectious Diseases*, 30(1), 104801. https://doi.org/10.1016/j.bjid.2026.104801

[22] Zitzler, E., Laumanns, M., Thiele, L. (2001). "SPEA2: Improving the strength Pareto evolutionary algorithm". *TIK Report*, 103, ETH Zurich. https://doi.org/10.3929/ethz-a-004284029

Author Bio-sketch

Islem Bennadja is a PhD candidate in the Department of Operational Research, University of Science and Technology Houari Boumediene (USTHB), Algeria. His research focuses on multi-objective optimal control and its applications in epidemic modeling and complex dynamical systems. Corresponding author. Email: ibennadja@usthb.dz

Omar Kebiri is a PhD researcher in the Department of Stochastics and its Applications, Brandenburg University of Technology Cottbus-Senftenberg, Germany. His research focuses on stochastic optimal control and its applications in molecular dynamics, finance, and epidemic modeling.

Djamal Chaabane is a Professor of Mathematics in the Department of Operational Research, University of Science and Technology Houari Boumediene (USTHB), Algeria. His research focuses on multi-objective optimization, decision support systems, stochastic programming, and combinatorial optimization.